JACS
JOURNAL OF THE AMERICAN CHEMICAL SOCIETY
Article
pubs.acs.org/JACS

Twisted Thiophene-Based Chromophores with Enhanced Intramolecular Charge Transfer for Cooperative Amplification of Third-Order Optical Nonlinearity

Natasha B. Teran,[†] Guang S. He,[‡] Alexander Baev,[‡] Yanrong Shi,[⊥] Mark T. Swihart,[§] Paras N. Prasad,[*,‡,∥] Tobin J. Marks,[*,⊥] and John R. Reynolds[*,†]

[†]School of Chemistry and Biochemistry, School of Materials Science and Engineering, and Center for Organic Photonics and Electronics, Georgia Institute of Technology, Atlanta, Georgia 30332, United States

[‡]The Institute for Lasers, Photonics and Biophotonics, [§]Department of Chemical and Biological Engineering, and [∥]Department of Chemistry, University at Buffalo (The State University of New York), Buffalo, New York 14260, United States

[⊥]Department of Chemistry and Materials Research Center, Northwestern University, Evanston, Illinois 60208, United States

Supporting Information

ABSTRACT: Exploiting synergistic cooperation between multiple sources of optical nonlinearity, we report the design, synthesis, and nonlinear optical properties of a series of electron-rich thiophene-containing donor−acceptor chromophores with condensed π-systems and sterically regulated inter-aryl twist angles. These structures couple two key mechanisms underlying optical nonlinearity, namely, (i) intramolecular charge transfer, greatly enhanced by increased electron density and reduced aromaticity at chromophore thiophene rings and (ii) a twisted chromophore geometry, producing a manifold of close-lying excited states and dipole moment changes between ground and excited states that are nearly twice that of untwisted systems. Spectroscopic, electrochemical, and nonlinear Z-scan measurements, combined with quantum chemical calculations, illuminate relationships between molecular structure and mechanisms of enhancement of the nonlinear refractive index. Experiment and calculations together reveal ground-state structures that are strongly responsive to the solvent polarity, leading to substantial negative solvatochromism ($\Delta\lambda \approx 10^2$ nm) and prevailing zwitterionic/aromatic structures in the solid state and in polar solvents. Ground-to-excited-state energy gaps below 2.0 eV are obtained in condensed π-systems, with lower energy gaps for twisted versus untwisted systems. The real part of the second hyperpolarizability in the twisted structures is much greater than the imaginary part, with the highest twist angle chromophore giving $|\mathrm{Re}(\gamma)/\mathrm{Im}(\gamma)| \approx 100$, making such chromophores very promising for all-optical-switching applications.

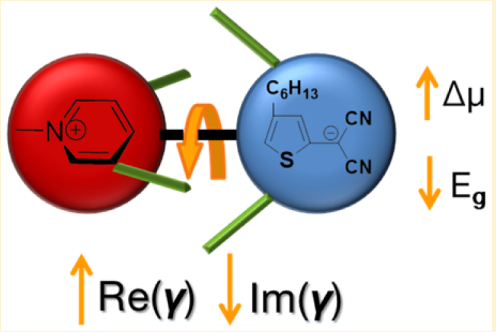

INTRODUCTION

Ever-growing demands for high-speed computing and telecommunication bandwidths have generated considerable interest in materials with large third-order optical nonlinearity for use in all-optical switching. Organic materials, with fast response times, low dielectric constants, facile processability, and exquisite tailorability, are especially promising candidates. The film-forming properties of many organics also simplify their integration into devices.[1−8]

The key performance metric for molecular third-order optical nonlinearity in organic materials is the microscopic second hyperpolarizability, γ, for which a sum-over-states expression is given by eq S1 in the Supporting Information. Often however, this infinite sum is truncated to include only a few essential states that make dominant contributions. A simplification of the sum-over-states approach to microscopic polarizabilities under nonresonant conditions, as given in the three-level model for γ below, provides insights into possible mechanisms for its enhancement:[5,6]

$$\gamma \propto \frac{M_{ge}^{\ 2}\Delta\mu^2}{E_{ge}^{\ 3}} - \frac{M_{ge}^{\ 4}}{E_{ge}^{\ 3}} + \frac{M_{ge}^{\ 2}}{E_{ge}^{\ 2}}\frac{M_{ee'}^{\ 2}}{E_{ge'}} \quad (1)$$

Here, M_{ge}, $M_{ge'}$, and $M_{ee'}$ are transition dipole moments between ground (g) and excited (e, e′) states, $\Delta\mu$ is the difference between ground-state and excited-state dipole moments ($\Delta\mu = \mu_e - \mu_g$), and E_{ge} and $E_{ge'}$ are transition energies between the ground state and close-lying excited states. Many approaches have been explored to maximize γ, mainly using highly conjugated structures that provide delocalized π-electrons and strong coupling between electronic and geometric structures.[5,9−11] The design of nonlinear optical (NLO) chromophores involves minimizing the transition energies in the denominators of eq 1 (for the resonant case, see eq S1), while maximizing the dipole moment change and/

Received: November 29, 2015
Published: May 27, 2016

DOI: 10.1021/jacs.5b12457
J. Am. Chem. Soc. 2016, 138, 6975−6984

or the transition dipoles in the numerators.[1] Prior design strategies include increasing the π-conjugation length,[12] end-capping π-systems with electron-donating and -accepting units,[13,14] and modulating bond length alternation (BLA).[15,16] These approaches rely to a great extent on expanding the π-electron system to enhance performance, which introduces synthetic complexity, chemical, photochemical, and thermal instability, and decreased transparency at visible and telecommunication wavelengths.[17]

The recent approach of Albert et al.[18,19] uses twisted intramolecular charge transfer (TICT) to reduce conjugation between the donor and acceptor fragments by deliberately twisting the intervening π-electron system. Molecules of this type are termed *tictoid* chromophores. Twisting the π-system enhances charge separation, creating an aromatically stabilized zwitterionic ground state, and hence inducing a large dipole moment change upon excitation. In the context of the three-level model embodied by eqs 1 and S1, this should increase the nonlinearity through the $\Delta\mu$-containing term. In addition, the existence of a dense manifold of low-lying excited states has been shown to provide a second mechanism of enhancement through the resonant denominator in eq S1.[18,19] Exceptionally large second- and third-order NLO responses have been realized in tictoid systems such as the TMC chromophores reported by the Marks group.[20−22]

In the present study, we demonstrate cooperative enhancement of third-order nonlinearity via incorporation of an electron-rich thiophene ring in the donor fragment of condensed tictoid donor−acceptor systems. This introduces the reduced delocalization energy and increased electron density of five-membered heteroaromatics into twisted chromophores.[23] On the acceptor fragment, we explore the effects of annelating arene rings onto the pyridine backbone,[24] allowing modulation of the acceptor strength, and the balance between aromatic vs quinoidal contributions to the π-system. Additionally, the inter-aryl twist angle is modulated by the number of substituents in the pseudo-*ortho* positions. These new chromophores allow us to explore the consequences of significant structural variations, while maintaining a condensed donor−acceptor π-system. The results demonstrate small ground-to-excited-state energy gaps, enhanced dipole moment changes (as evidenced by negative solvatochromic behavior), and closely spaced excited states, leading to second hyperpolarizabilities up to 10 times those of previously reported condensed twisted systems in the chromophore with the highest twist angle.[20,22]

RESULTS AND DISCUSSION

To fully understand the effects of introducing the electron-rich thiophene ring in TICT chromophores, and of increasing annelation in quinoline and acridine rings, the family of chromophores shown in Chart 1 was synthesized and fully characterized. Structural characteristics were studied via NMR and FTIR spectroscopy, aided by DFT calculations, with a focus on determining the contribution of the zwitterionic/aromatic (ZA) and neutral-quinoidal (NQ) forms to the ground-state structures of the chromophores. Optical absorption spectroscopy was used to further explore the degree of charge separation in both the ground and excited states of these chromophores, enabling measurement of key parameters such as $\Delta\mu$, M_{ge}, and E_{ge} (from the onset of optical absorption and supported with electrochemical measurements). The NLO response, specifically the real and imaginary parts of γ, the

Chart 1. Resonance Forms of Tictoid Thiophene-Based Chromophores

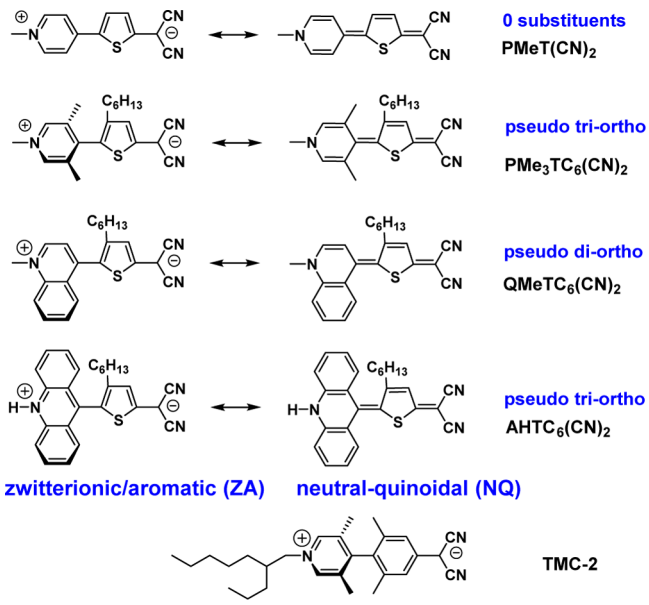

second-order refractive index n_2, and the corresponding one-photon figure-of-merit W (ratio of n_2 to the linear loss per unit length;[25] see the Supporting Information for the definition) and two-photon figure-of-merit T (ratio of the nonlinear loss per unit length to n_2;[26] see the Supporting Information for the definition) were then characterized by Z-scan experiments. Finally, DFT calculations allow mechanistic interpretation and a deeper understanding of the experimental observations.

Chromophore Design and Synthesis. Two key structural design modifications were implemented here relative to the previously studied TMC tictoid chromophores: on the donor side, the effects of replacing an arene ring with an electron-rich, less aromatic thiophene ring, and, on the acceptor side, the effects of annelating arene rings to the pyridinium core, thereby incrementally increasing the acceptor strength. In replacing the arene ring in the donor fragment of the first-generation TMC chromophores with a thiophene, the increased electron density is expected to alter the HOMO energy, the extent of ZA charge separation, and the degree of intramolecular charge transfer from the ground state to the excited state. Simultaneously, the lower delocalization energy of the thiophene ring, relative to an arene, is expected to alter the degree of donor−acceptor π-delocalization. This is expected to result in destabilization of the ZA state, while stabilizing the NQ state, thereby affecting the ground-to-excited-state energy gap. On the acceptor side, successive introduction of annelated arene rings to the pyridinium core should increase the electron-accepting strength in the order pyridine/3,5-lutidine < quinoline < acridine. The principal effect of annelation should be increased NQ structure stabilization, with annelated rings enhancing the aromatic character (Chart 1). Because the tictoid design paradigm relies on sterically constraining the conjugation across a donor- and acceptor-modified biaryl system, the inter-aryl torsion angle is a crucial structural feature in these thiophene-based chromophores. Replacing a six-membered arene ring with a five-membered thiophene ring should also relax steric repulsion about the inter-aryl bond, and limit the maximum number of substituents to a pseudo-tri-*ortho* pattern. Substituents change from none for pyridine to one for quinoline and to two for 3,5-

DOI: 10.1021/jacs.5b12457
J. Am. Chem. Soc. 2016, 138, 6975−6984

Scheme 1. Synthesis of Chromophores

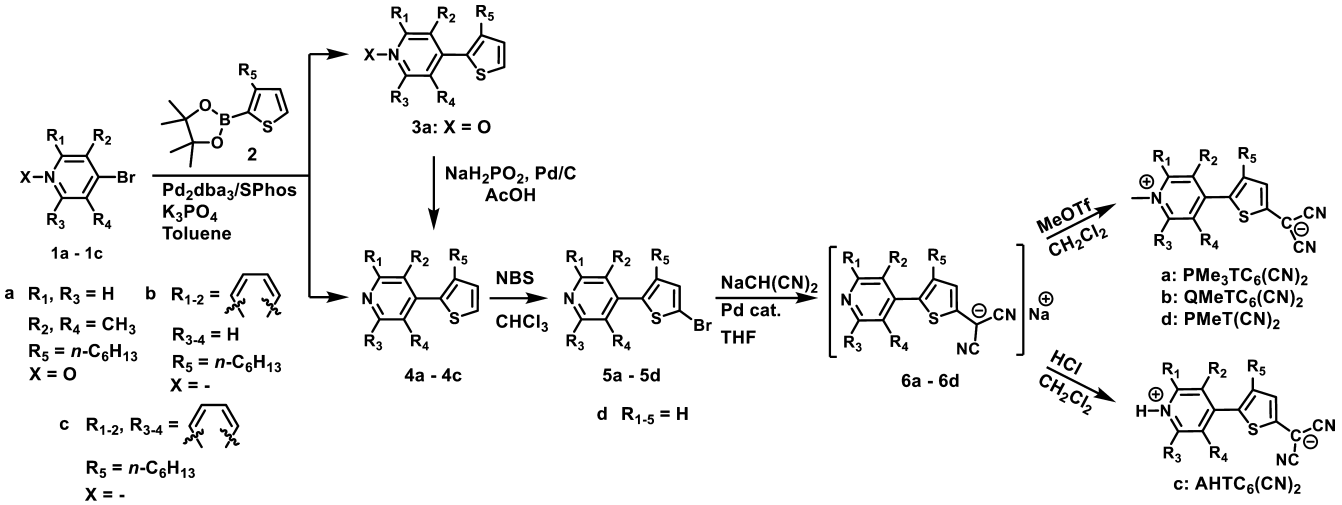

lutidine and acridine. Also, the 3,5-lutidine CH_3 substituents are expected to exert greater steric repulsion than a CH_2 group at the *ortho* position of the pyridine ring in quinoline and acridine.

As all these structural modifications are applied, the sterically controlled torsion angle and the chromophore electronic distribution are simultaneously influenced. To isolate these two effects, $PMe_3TC_6(CN)_2$ and $PMeT(CN)_2$,[27] which have identical donor and acceptor cores and the same π-system, but drastically different inter-aryl steric bulk, are compared. The interplay of electronic and steric effects is considered in analyzing the experimental data.

The synthetic approach to obtain the new tictoid thiophene-based chromophores is shown in Scheme 1. While the desired sterically driven inter-aryl twist presents a clear synthetic challenge, recent developments in cross-coupling methodologies have afforded high-yield carbon−carbon bond formation between sterically hindered substrates.[28−30] To improve atom economy and reduce the number of synthetic steps, we combined a key inter-aryl torsion element with a needed solubilizing group by utilizing a 3-hexyl-substituted thiophene in the donor fragment. With the commercial availability of the 2-boronic acid pinacol ester derivative of this compound, Suzuki chemistry was selected as the biaryl cross-coupling methodology. For the chromophores presented here, the electron-rich and sterically bulky ligand dicyclohexyl(2′,6′-dimethoxy-[1,1′-biphenyl]-2-yl)phosphane (SPhos)[31] enabled the couplings in high yields. The negative-charge-bearing dicyanomethanide group was installed through a Pd-catalyzed coupling with malononitrile. The positive charge was then obtained by quaternization of the arene N with methyl triflate or acid treatment. Further details of the synthetic approach and procedures can be found in Section II of the Supporting Information.

Tictoid Chromophore Properties from FTIR, NMR, Optical Spectroscopy, and Quantum Chemical Calculations. The electronic structures of tictoid chromophores can be described by a balance of ZA and NQ resonance forms (Chart 1). The resultant optoelectronic properties depend on the relative contribution of each form to the ground and excited states. Here, spectroscopic and computational investigations were combined to provide a clear understanding of the relative contributions of the ZA and NQ forms. In particular, the sensitivity of the structural and electronic properties of the thiophene-based chromophores to their solvent environment showed good agreement between experiment and theory, allowing confident interpretation of the results.

FTIR spectra of the chromophores and their sodium salt precursors **6a−d**, taken as powders pressed onto a ZnSe crystal plate, are shown in Figure S1 (Supporting Information, Section III). All chromophores have ZA structures in the solid state, based on $\nu(C{\equiv}N)$ frequencies (<2200 cm^{-1}) and kinematic coupling. $PMe_3TC_6(CN)_2$ has the lowest frequency $\nu(C{\equiv}N)$ stretches and strongest kinematic coupling, reflecting substantial negative charge concentration in the $C(C{\equiv}N)_2$ group. The $\nu(C{\equiv}N)$ frequency increases in $QMeTC_6(CN)_2$ and $AHTC_6(CN)_2$, with the highest frequency observed in $PMeT(CN)_2$. The $\nu(C{\equiv}N)$ kinematic coupling also falls markedly in the latter three chromophores, indicating greater charge delocalization through the π-system.[32] These results follow the expected trend for increasing NQ stability with lower inter-aryl steric crowding, and increasing acceptor core annelation: $PMe_3TC_6(CN)_2 \ll QMeTC_6(CN)_2 < AHTC_6(CN)_2 \approx PMeT(CN)_2$. Moreover, $PMe_3TC_6(CN)_2$ and $PMeT(CN)_2$ have substantially different vibrational spectra despite their similar π-systems due to the disrupted conjugation induced by the pseudo-tri-*ortho* substitution in $PMe_3TC_6(CN)_2$.

Chromophore solution structural properties were probed by ^1H and ^{13}C NMR spectroscopy. The key ^1H NMR resonances are summarized in Tables S1−S4 and Figure S2. The thiophene 3-H peaks for $PMe_3TC_6(CN)_2$, $QMeTC_6(CN)_2$, and $PMeT(CN)_2$ occur upfield due to electron donation from the negatively charged dicyanomethanide group. In contrast, the thiophene 3-H peak of $AHTC_6(CN)_2$ occurs in a relatively downfield region, indicating an NQ character greater than that of the other chromophores. The *N*-methyl protons of $PMe_3TC_6(CN)_2$, $QMeTC_6(CN)_2$, and $PMeT(CN)_2$ are observed in a downfield region, and a slight to moderate downfield shift of the pyridinium ring protons is observed in all chromophores due to the (partial) positive charge on the ring N. Solvent-dependent ^1H NMR spectroscopy (Supporting Information, Section III and Tables S1−S4) also support the ZA structure and greater charge localization in $PMe_3TC_6(CN)_2$, and increased NQ character in $QMeTC_6(CN)_2$, $AHTC_6(CN)_2$ (in less polar solvents; ZA structure in polar acetone-d_6), and $PMeT(CN)_2$.

DOI: 10.1021/jacs.5b12457
J. Am. Chem. Soc. 2016, 138, 6975−6984

Quantum chemical calculations of the structural and electronic properties of the thiophene-based chromophores were carried out, as shown in Figure 1, which illustrates their

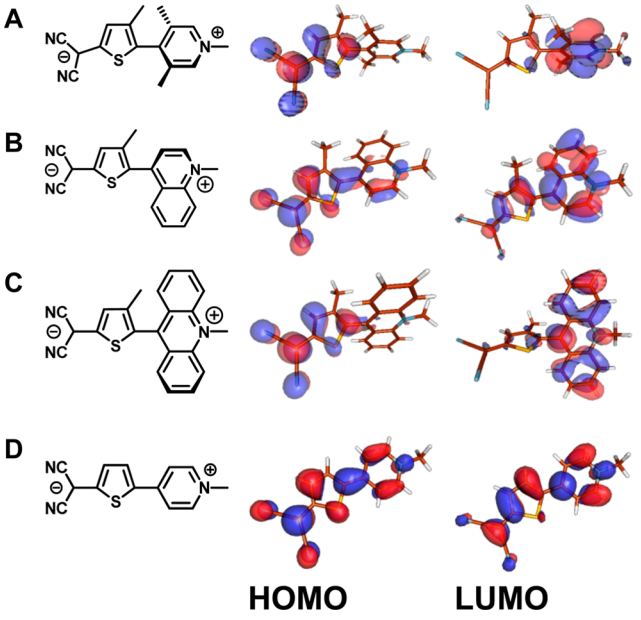

Figure 1. Pictorial representations of the HOMOs and LUMOs of (A) $PMe_3TC_6(CN)_2$, (B) $QMeTC_6(CN)_2$, (C) $AHTC_6(CN)_2$, and (D) $PMeT(CN)_2$.

calculated frontier molecular orbitals. The structural properties calculated for these chromophores (Table 1) show twist angles (θ) that reflect the degree of inter-aryl steric substitution. Note that the geometries, optimized by the Hartree−Fock method in vacuum, show a much less pronounced twist around the inter-aryl bond compared to optimization carried out with the polarizable continuum model (PCM) representing a polar medium ($CHCl_3$). $CHCl_3$ has been chosen as a representative low-polarity solvent for calculating the geometries of the chromophores. Its modest dielectric constant (4.81) produces a less intense reaction field than a more polarizable solvent in the polarized continuum methodology, which saves computational resources. Earlier calculations of a similar twist-motif system, TMC-2, showed that the inter-ring torsion angle changed negligibly between calculations using $CHCl_3$ or DCM as the polarizable dielectric medium.[21] This allows comparisons to be made between calculations done in $CHCl_3$ and experiments done in DCM (vide infra).

The results in Table 1 show that calculations in vacuo do not render correct twist geometries and greatly overestimate the energy gaps. The calculated energy gaps (E_g) in $CHCl_3$ are less than half the values in vacuum for the most twisted systems, $PMe_3TC_6(CN)_2$ and $AHTC_6(CN)_2$, indicating low-lying excited states for the twisted chromophores. The computed ground-state dipole moments (μ_g) are significantly larger in $CHCl_3$ versus vacuum by factors of nearly 2 and 3 for $PMe_3TC_6(CN)_2$ and $AHTC_6(CN)_2$, respectively. Thus, the calculations also support the assignment of a ZA structure in polar solvents.

The solution optical absorption spectra of the chromophores reflect the structural picture provided by NMR spectroscopy and quantum chemical calculations. All chromophores have broad donor−acceptor intramolecular charge transfer (ICT) features in the 400−1000 nm region (Figure 2, Table 2), which are red-shifted despite the small size of the π-system.

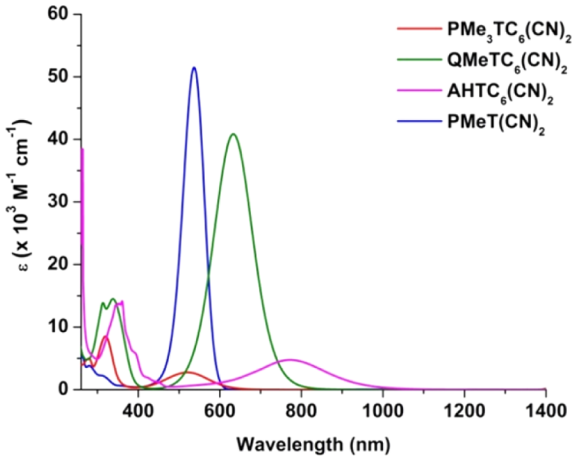

Figure 2. Optical absorption spectra of the present chromophores in methanol.

$PMe_3TC_6(CN)_2$, $QMeTC_6(CN)_2$, and $AHTC_6(CN)_2$ also show high-energy absorptions assignable to the respective donor and acceptor intra-ring excitations, as predicted for tictoid chromophores.[19] The ICT peaks for $PMe_3TC_6(CN)_2$ and $AHTC_6(CN)_2$ have weaker molar extinction coefficients (ε) than the intra-ring excitations, due to modest overlap of donor and acceptor orbitals (Figure 1A,C). In $QMeTC_6(CN)_2$ and $PMeT(CN)_2$ the coefficients are large due to their less sterically hindered inter-aryl bond allowing significant orbital overlap (Figure 1B,D).

Theoretical calculations have shown that the chromophore twist angles vary with the polarity of the medium. Because the extent of twist dictates the degree of overlap between the donor and the acceptor fragment orbitals, the linear optical properties are also expected to vary with the solvent. Indeed, the λ_{max} and ε of the ICT bands shift with the solvent polarity (Figure S3), indicating variation of the electronic distribution and state energies. In contrast, a weaker response to solvent polarity is observed for the intra-subfragment transitions (Figure S4). Similar solvent polarity effects on electronic properties have been previously reported in other tictoid systems.[20,36]

$PMe_3TC_6(CN)_2$, $QMeTC_6(CN)_2$, and $PMeT(CN)_2$ show negative solvatochromic behavior (Figure S3), indicating that the ZA limit is a better representation of their ground-state structure, whereas the NQ form is likely a major contributor to the excited-state structure. For $AHTC_6(CN)_2$, the NQ form predominates in less polar solvents, while the ZA form predominates in more polar solvents, leading to solvatochromic reversal. This striking change was also observed in its FTIR and NMR spectra. The pronounced solvatochromic effect observed for $PMe_3TC_6(CN)_2$ and $AHTC_6(CN)_2$ indicates that a larger change in dipole moment ($\Delta\mu$) between the ground and excited states occurs for these chromophores. Because no fluorescence emission is observed from the ICT transition in these tictoid chromophores, the McRae equation[33−35] provides a simple relationship to estimate $\Delta\mu$ from the solvatochromic shifts in absorption maxima via linear regression analysis (see the Supporting Information, Section IV, Figure S5). The results are shown in Table 2. The significant twist present in $PMe_3TC_6(CN)_2$ and $AHTC_6(CN)_2$ allows greater charge localization in the donor and acceptor rings, increasing $\Delta\mu$.

DOI: 10.1021/jacs.5b12457
J. Am. Chem. Soc. 2016, 138, 6975−6984

Table 1. Computed Structural and Electronic Properties of Twisted Thiophene-Based Chromophores

	vacuum			polar medium ($CHCl_3$)		
chromophore	θ (deg)	E_g (eV) (wavelength, nm)	μ_g (D)	θ (deg)	E_g (eV) (wavelength, nm)	μ_g (D)
$PMe_3TC_6(CN)_2$	40	2.5 (496)	20.8	74	1.2 (1033)	35.4
$QMeTC_6(CN)_2$	18	2.8 (443)	15.8	40	2.0 (620)	32.1
$AHTC_6(CN)_2$	10	3.1 (400)	12.0	68	1.1 (1127)	33.5
$PMeT(CN)_2$				0	2.7 (459)	21.0

Table 2. Optical Absorption Properties (λ_{max}, ε, $\Delta\lambda_{max}$, M_{ge}, $\Delta\mu$, $E_{g,opt}$) and Electrochemically Derived Properties (HOMO Level, E_H, and Energy Gap, $E_{g,ec}$) of the Intramolecular Charge Transfer in the Thiophene-Based Chromophores

	λ_{max}[a] (nm) (ε, M^{-1} cm^{-1})				M_{ge}[e] (D)			$E_{g,opt}$[g] (eV) (wavelength, nm)				
chromophore	ACN	DCM	$CHCl_3$	$\Delta\lambda_{max}$[c] (nm)	ACN	DCM	$\Delta\mu$[f] (D)	ACN	DCM	$CHCl_3$	E_H[h] (eV)	$E_{g,ec}$[h] (eV)
$PMe_3TC_6(CN)_2$	540 (5260)	634 (12100)	668 (10200)	150	3.2	5.2	−7.0	1.92 (646)	1.69 (734)	1.55 (801)	−4.97	1.62
$QMeTC_6(CN)_2$	646 (43500)	683 (52200)	686 (69900)	53	8.6	10	−2.0	1.67 (743)	1.59 (780)	1.52 (815)	−5.07	1.29
$AHTC_6(CN)_2$	803 (2800)	577 (644)	578 (588)	248[d]	2.8[d]	2.2[d]	8.5	1.23 (1008)	1.19 (1042)	1.19 (1042)	−4.89	0.93
$PMeT(CN)_2$	545 (73000)	589 (29500)	600 (23400)	63[d]	8.8		−3.6	2.09 (593)	2.01 (618)	1.97 (629)	−5.20	1.82
TMC-2[i]	472	569 (1840)		170				2.16			−5.49	

[a]Assigned to ICT excitation. [b]Assigned to the lowest energy vibrational sub-band. [c]Taken as the difference between the most red-shifted and most blue-shifted spectra. [d]Disregards changes in the spectral shape. [e]Calculated from

$$|M_{ge}|^2 = \frac{3 \ln 10 hc\varepsilon_0}{2\pi^2 N_A} \int_{\bar{\nu}}^{\varepsilon} d\nu$$

. [f]Calculated from eqs S2−S4 (see the Supporting Information, Section IV).[33−35] [g]Calculated from the lower energy onset of absorption in each solvent. [h]All values referenced to the ferrocene $E_{1/2}$ = 0.067 V vs Ag/Ag^+ in CH_3CN, and reported relative to that in vacuum (−5.1 eV). [i]Values from ref 20.

The stronger donor thiophene ring in $PMe_3TC_6(CN)_2$ also allows it to achieve nearly the same $\Delta\lambda_{max}$ as TMC-2,[20] despite the lower inter-aryl steric bulk.

The transition dipole moments (M_{ge}) for the chromophores, estimated from the area under the ICT peak (Figure S6), and summarized in Table 2, are moderate in chromophores with larger twist angles, $PMe_3TC_6(CN)_2$ and $AHTC_6(CN)_2$, in agreement with the moderate ground- and excited-state wave function overlap determined from quantum chemical calculations. On the other hand, less sterically hindered chromophores, $QMeTC_6(CN)_2$ and $PMeT(CN)_2$, have larger M_{ge}, due to the greater conjugation across the donor and acceptor subfragments.

The calculated (Table 1, in $CHCl_3$) and experimental (Table 2, $E_{g,opt}$) ground-to-excited-state energy gaps for all thiophene-based chromophores are below 2.0 eV, and smaller than that of TMC-2. This is attributed to the electron-richness of the thiophene ring, which leads to raised HOMO energies (Table 2, E_H from electrochemistry, Supporting Information, Section V, Figure S7, Table S6).

Nonlinear Optical Properties from Quantum Chemical Calculations. From the viewpoint of NLO applications, a useful organic chromophore should exhibit either: (i) an exceptional light-intensity-dependent nonlinear absorption for optical power limiting or (ii) an exceptional intensity-dependent nonlinear refractive index change for high-speed optical switching, data storage, and transmission applications. The nonlinear refractive index change can be quantified via the real part of the second hyperpolarizability, Re(γ), which must be large for practical applications. Simultaneously, the attenuations from both linear (one-photon) and nonlinear (two-photon) absorption should also be as small as possible. The former is characterized by the W parameter, and the latter by the T parameter. The nonlinear absorption is directly related to the imaginary part of the second hyperpolarizability, Im(γ).

Calculations of Re(γ) and the W and T parameters were performed for all studied thiophene-based chromophores. The results of time-dependent DFT calculations are summarized in Table 3. The systems with the greatest twist (in $CHCl_3$), $PMe_3TC_6(CN)_2$ and $AHTC_6(CN)_2$, show the largest values of Re(γ) at 1550 nm, a telecommunication wavelength. Both structures have low-lying first excited states (Table 2) with excitation wavelengths of 1033 and 1127 nm, respectively, and a manifold of closely spaced upper excited states (Figure S8). Stronger quasi-resonant linear absorption (residual absorption at wavelengths corresponding to the edge of the absorption band) in $AHTC_6(CN)_2$ results in a lower W parameter (Table 3). However, the more energetic second excited state of $AHTC_6(CN)_2$ (418 nm excitation) leads to lower quasi-resonant two-photon absorption, and a lower T parameter value, than in $PMe_3TC_6(CN)_2$ (539 nm excitation). In comparison, the chromophore with a smaller twist, $QMeTC_6(CN)_2$, has a higher lying first excited state with excitation at 620 nm, accompanied by a much lower value and opposite sign of Re(γ), and a relatively strong two-photon absorption, resulting in a very large T parameter (Table 3).

The fact that the two-photon excitation of $QMeTC_6(CN)_2$ at 1550 nm is more resonant than those of $PMe_3TC_6(CN)_2$ and

DOI: 10.1021/jacs.5b12457
J. Am. Chem. Soc. 2016, 138, 6975−6984

Table 3. Real Part of the Twisted Thiophene-Based Chromophore Second Hyperpolarizability, γ_{av}, at 1550 nm[a]

	vacuum geometry			$CHCl_3$ geometry			
chromophore	γ_{av} (10^5 au)	γ_{av} (10^{-36} esu)	$T = \alpha_2\lambda/n_2$	γ_{av} (10^5 au)	γ_{av} (10^{-36} esu)	$T = \alpha_2\lambda/n_2$	$W = n_2 I/\alpha_1\lambda$ (I = 10 MW/cm^2)
$PMe_3TC_6(CN)_2$	−0.046	−2.32	−136.57	−179.3	−9079	2.46	2.45
$QMeTC_6(CN)_2$	1.19	59.9	0.05	0.005	0.25	10^4	10^{-4}
$AHTC_6(CN)_2$	2.31	116	0.02	−142.5	−7216	0.4	0.93
$PMeT(CN)_2$				−0.24	−12	48.81	$\sim 10^{-6}$

[a]The nonresonant α_2 is estimated with inhomogeneous broadening of 0.5 eV.

Table 4. Real Part of the Second Hyperpolarizability, γ_{av} (10^5 au) (10^{-36} esu), vs the Excitation Wavelength[a]

chromophore	775 nm	1000 nm	1300 nm	1550 nm
$PMe_3TC_6(CN)_2$	302.47 (15316)	resonant	−509.2 (−25784)	−179.3 (−9079)
$QMeTC_6(CN)_2$	−68.7 (−3479)	−26.1 (−1322)	12.65 (641)	0.005 (0.25)
$AHTC_6(CN)_2$	652.7 (33051)	resonant	289.9 (14680)	−142.5 (−7216)
$PMeT(CN)_2$	−3.07 (−155)	0.58 (29)	−0.237 (−12)	−0.243 (−12)

[a]"Resonant" indicates numerical divergence, leading to nonphysical values.

$AHTC_6(CN)_2$ makes this particular chromophore a much poorer all-optical-switching medium at this wavelength. However, it might in principle perform better at a different wavelength. To investigate this possibility, Re(γ) was computed for all chromophores at 1550, 1300, 1000, and 775 nm (Table 4). Even though Re(γ) of $QMeTC_6(CN)_2$ increases at wavelengths shorter than 1550 nm, it is still outperformed by $PMe_3TC_6(CN)_2$ and $AHTC_6(CN)_2$ at all wavelengths.

At 775 nm, $AHTC_6(CN)_2$ outperforms $PMe_3TC_6(CN)_2$, and at 1300 nm, they have opposite signs for Re(γ), corresponding to self-focusing (positive sign) and self-defocusing (negative sign), respectively. Note that, at 1000 nm, the excitation is too close to the one-photon resonance of both $PMe_3TC_6(CN)_2$ and $AHTC_6(CN)_2$, resulting in numerical divergence and nonphysical values. Proper damping must be introduced to compute γ near resonance.

Relative to tictoid molecules, the first excited state of nontwisted $PMeT(CN)_2$ is of higher energy (459 nm excitation wavelength) and has a lower dipole moment (Table 1). The Re(γ) of this system is also far lower than that of all the tictoid systems (Table 4). Although the value is greater than that of $QMeTC_6(CN)_2$ at one particular wavelength (1550 nm), the gradient of Re(γ) is still much smaller for $PMeT(CN)_2$.

These results clearly demonstrate the effect on Re(γ) of the sterically induced twist around the inter-aryl bond. The importance of the twisted geometry in tictoid systems is further demonstrated by comparison of the computed Re(γ) at different wavelengths for the vacuum and $CHCl_3$ geometries of the most sterically hindered system, $PMe_3TC_6(CN)_2$ (Table S7). With the geometry optimized in vacuum, both the Re(γ) and its gradient are far smaller than for the geometry optimized in a polar medium. These twisted geometry effects on NLO properties can be attributed to (1) large dipole moment changes upon excitation and (2) a manifold of closely spaced excited states (Figure S8),[19,37,38] accumulating the nonlinear response of the tictoid systems in a narrow spectral range (summation over excited states in eq S1).

Nonlinear Optical Properties from *Z*-Scan Measurements. For an isotropic optical medium, the third-order nonlinearity is the lowest order nonlinearity possible. It is quantified by the third-order nonlinear susceptibility $\chi^{(3)}$, a wavelength-dependent macroscopic parameter that is related to the microscopic coefficient γ by a multiplicative factor of the number density (N_0) and a local field correction factor.

If the frequency ω of the input laser field is far from resonance (one- or two-photon) with frequency ω_{ge}, $\chi^{(3)}$ will reflect a real-valued nonresonant contribution (nonresonant background), whereas if the laser frequency ω is near a transition frequency of the given medium, $\chi^{(3)}$ will include the nonresonant background and the resonant (two-photon, accounted for by the first and second terms in eq S1, or one-photon, accounted for by all three terms in eq S1, respectively) contribution. Thus, under resonant conditions,

$$\chi^{(3)} = \chi^{(3)}_{nonr} + \chi^{(3)}_{res} \tag{2}$$

The resonant $\chi^{(3)}$ is then a complex quantity. For example, at two-photon (2p) resonance it can be written as,

$$\chi^{(3)}_{res} \propto N_0 \frac{1}{(\omega_{ge} - 2\omega) - i\Gamma_{ge}} \tag{3}$$

where ω_{ge} is the central frequency of a dipole-allowed two-photon transition of the medium and Γ_{ge} is the spectral half-width of the corresponding transition (see also eq S1). The overall $\chi^{(3)}$ can be expressed as the sum of its real and imaginary parts:

$$\begin{aligned}\chi^{(3)} &= \mathrm{Re}(\chi^{(3)}) + i\mathrm{Im}(\chi^{(3)}) \\ &= (\chi^{(3)}_{nonr} + \mathrm{Re}(\chi^{(3)}_{res})) + i\mathrm{Im}(\chi^{(3)}_{res})\end{aligned} \tag{4}$$

As discussed above for γ, the real part determines the intensity-dependent refractive index change of the medium, while the imaginary part determines the nonlinear (two-photon) absorption. These nonlinear properties are both measured using the *Z*-scan method. Two-photon absorption is obtained from open-aperture *Z*-scan measurements, while the nonlinear refractive index change is obtained from closed-aperture *Z*-scan measurements. Here, *Z*-scan measurements were primarily conducted at two telecommunication wavelengths, ~800 and ~1300 nm. The ~800 nm, ~160 fs laser beam was from a Ti:sapphire oscillator/amplifier system, whereas the ~1300 nm, ~160 fs input beam was from an optical parametric generator system (see the Supporting Information, Section I).

In an absolute *Z*-scan experiment, to extract the values of the real and imaginary parts of $\chi^{(3)}$, one must evaluate the local intensity of a focused laser beam and its changes with the *Z*-position, which introduces relatively large uncertainties.[39] In

DOI: 10.1021/jacs.5b12457
J. Am. Chem. Soc. 2016, 138, 6975−6984

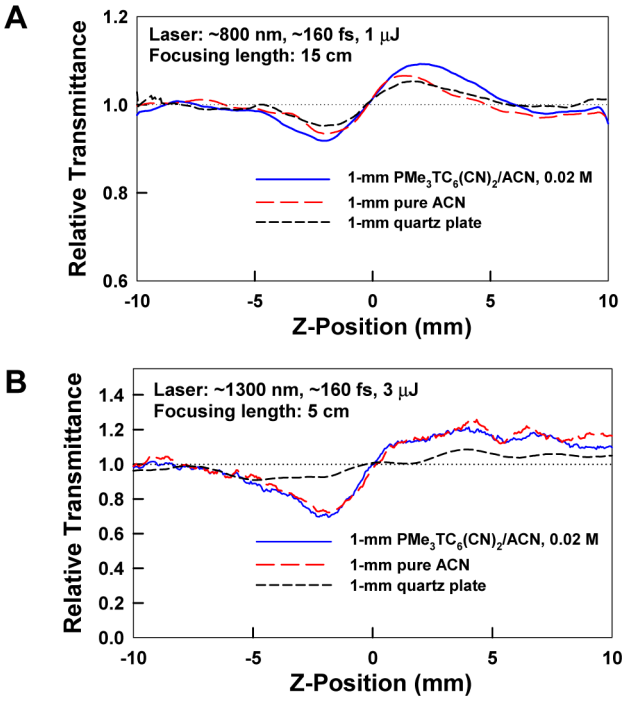

Figure 3. Closed-aperture *Z*-scan measurements on $PMe_3TC_6(CN)_2$ in ACN at ~800 nm (A) and ~1300 nm (B).

contrast, by using a quartz glass plate (the $\chi^{(3)}$ value for which is well-known) as a standard sample in a comparative *Z*-scan measurement, the relative uncertainty of data extraction can be remarkably reduced.[40]

Z-scan measurements were performed on $PMe_3TC_6(CN)_2$ and $QMeTC_6(CN)_2$, as representative high-twist and low-twist systems, respectively. Unfortunately, *Z*-scan measurements could not be performed for $AHTC_6(CN)_2$ due to its limited solubility, and low-energy onset of absorption. Solvents were selected on the basis of a combination of solubility and minimization of overlap between the solvent-specific linear absorption spectra of the chromophore and the *Z*-scan measurement wavelength. Thus, DCM and ACN were used for $PMe_3TC_6(CN)_2$, while benzyl alcohol was used for $QMeTC_6(CN)_2$. The use of DCM for $PMe_3TC_6(CN)_2$ enables comparison with the results of calculations (performed in $CHCl_3$). The data are shown in Figures 3−5 and Figure S9. Extracted parameters are collected in Table 5. Where chromophore contributions are smaller than that of the solvent, parameters are given as maximum possible values.

Parts A and B of Figure 3 show closed-aperture *Z*-scan results with the 1 mm samples of quartz glass plate (standard sample), the pure ACN solvent, and the 0.02 M $PMe_3TC_6(CN)_2$ solution measured at laser wavelengths of ~800 and ~1300 nm, respectively, while parts A and B of Figure S9 present the corresponding open-aperture results. The laser pulse repetition rate for these measurements was ~30 Hz. The open-aperture *Z*-scan results show that the intensity-dependent nonlinear absorption is negligible at both wavelengths for the $PMe_3TC_6(CN)_2$ solution. In contrast, from the closed-aperture *Z*-scan curves shown in Figure 3A, the $PMe_3TC_6(CN)_2$ contribution to the induced refractive index change at ~800 nm is ~50% of that of the 1 mm quartz glass. The nonlinear refractive index coefficient for the latter is known to be $n_2(\text{quartz}) = 3 \times 10^{-7}$ cm^2/GW; therefore, the contribution of 0.02 M $PMe_3TC_6(CN)_2$ to the induced refractive index change should be $n_2' = 1.5 \times 10^{-7}$ cm^2/GW. From this, the contribution to $\text{Re}(\chi^{(3)})$ is 2.9×10^{-15} esu, and that to $\text{Re}(\gamma')$ is $\leq 2.4 \times 10^{-34}$ esu. At 1300 nm (Figure 3B), the contribution from 0.02 M $PMe_3TC_6(CN)_2$ to the induced refractive index change is far smaller than that of the pure solvent.

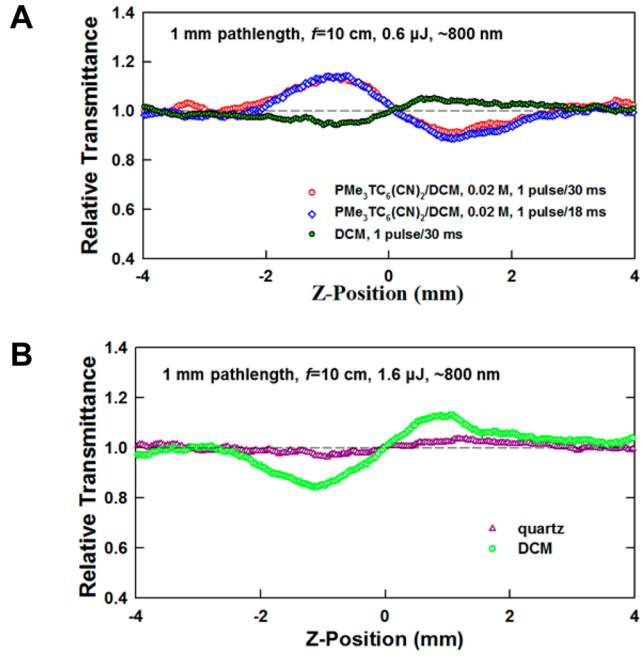

Figure 4. (A) Closed-aperture *Z*-scan measurements on $PMe_3TC_6(CN)_2$ in DCM at ~800 nm. (B) Comparison between 1 mm DCM and quartz glass plate at a higher pulse energy level.

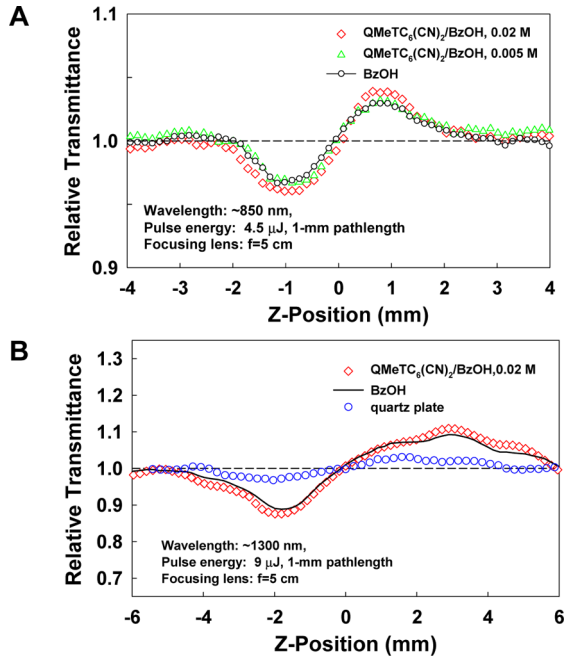

Figure 5. Closed-aperture *Z*-scan measurements of $QMeTC_6(CN)_2$ in BzOH at (A) ~850 nm and (B) ~1300 nm.

Figure 4A shows the closed-aperture *Z*-scan results (open-aperture results are shown in Figure S9C) for a 0.02 M $PMe_3TC_6(CN)_2$ solution in DCM at ~800 nm wavelength, obtained with two different laser pulse repetition rates. Their similarity excludes the possibility of thermal influence on the

DOI: 10.1021/jacs.5b12457
J. Am. Chem. Soc. 2016, 138, 6975−6984

Table 5. Third-Order Nonlinear Properties of $PMe_3TC_6(CN)_2$ and $QMeTC_6(CN)_2$ in Solution at 0.02 M Concentration (Experimental Uncertainty ±10%)

	$PMe_3TC_6(CN)_2$			$QMeTC_6(CN)_2$	
	ACN	ACN	DCM	BzOH	BzOH
wavelength (nm)	~800	~1300	~800	~850	~1300
n_2 contribution from solute (cm^2/GW)	1.5×10^{-7}	0.75×10^{-7}	-9×10^{-6}	3.2×10^{-7}	1.5×10^{-7}
Re(γ) (esu)	0.24×10^{-33}	$\leq 0.12 \times 10^{-33}$	-1.42×10^{-32}	0.50×10^{-33}	$\leq 0.24 \times 10^{-33}$
Im(γ) (esu)	$\leq 1.63 \times 10^{-35}$	$\leq 1.63 \times 10^{-35}$	$\leq 1.63 \times 10^{-35}$	$\leq 1.63 \times 10^{-35}$	$\leq 1.63 \times 10^{-35}$
T parameter	≤0.533	≤1.73	≤0.0089	≤0.283	≤1.08
W (at 10 MW/cm^2 level)	0.375×10^{-3}	0.115×10^{-3}	0.56×10^{-3}	0.706×10^{-3}	0.185×10^{-3}

Table 6. Comparison of Third-Order Nonlinear Parameters of Twisted π-Systems and Other Organic NLO Chromophores

	twisted π-system chromophores			other organic chromophroes		
	$PMe_3TC_6(CN)_2$ in DCM	Cy-TICT in DCM[22]	TMC-2 in DCM[21]	rhodamine B in ethanol[40]	cationic dye 1a in DCM[41]	ST1 in DCM[42]
wavelength (nm)	~800	~1305	~775	~800	1550	1064
Re(γ) (10^{-33} esu)	−14.2	−6.43	1.4	−1.0	−10	11.1
Im(γ) (10^{-35} esu)	≤1.63	58.8	3.43	30	1600	≤19.2
T parameter	≤0.0089	1.15	0.308			≤0.3

measurements. The chromophore contribution to the nonlinear refractive index change is $\Delta n(\text{solute}) \approx -4.7\Delta n(\text{DCM})$. Moreover, from Figure 4B, we see that $\Delta n(\text{DCM}) \approx 6.3\Delta n(\text{quartz})$. Therefore, the solute contribution is determined to be $n_2 \approx -30n_2(\text{quartz}) = 9 \times 10^{-6}$ cm^2/GW, from which the estimated real part of the molecular second hyperpolarizability is $\text{Re}(\gamma') = -1.42 \times 10^{-32}$ esu.

Figure 5 shows closed-aperture Z-scan results for 0.02 M and 0.005 M $QMeTC_6(CN)_2$ in BzOH at 850 and 1300 nm. The linear optical absorption spectrum of $QMeTC_6(CN)_2$ in this solvent (Figure S10) tails past 800 nm, precluding Z-scan measurements at 800 nm. At 850 and 1300 nm, the chromophore contribution to the induced (positive) refractive index change is small as evidenced by the small difference between the Z-scan curves for the pure solvent and the solution. Unfortunately, due to limited solubility of $QMeTC_6(CN)_2$ in BzOH, we could not make measurements at higher concentration where the separation between the curves would be greater. Nonetheless, we were still able to extract the contribution of the chromophore to n_2 from the small but measurable difference between the variation in transmission obtained for the pure solvent and solution. The relative deviation of Z-scan curves from unity, defined as the deviation of the curve for the solution divided by that for the solvent, was 20% at 850 nm and 9% at 1300 nm (Figure 5). The contribution of the solute to $\text{Re}(\chi^{(3)})$ was computed from these relative deviations. Because these are small relative differences, the relative uncertainty in the parameters determined from them is small. The absolute uncertainty, however, is limited, and thus, we can still make meaningful, semiquantitative comparisons between these results for $QMeTC_6(CN)_2$ and the results for $PMe_3TC_6(CN)_2$. The open-aperture Z-scan results at these two wavelengths once again indicate negligible nonlinear absorption within the experimental uncertainty and the system sensitivity. Note that, even though the measured contribution of the chromophore to $\text{Re}(\chi^{(3)})$ is an order of magnitude lower than that of the pure solvent, the corresponding second hyperpolarizability of a single chromophore molecule is still far greater than that of a single solvent molecule, as the chromophore concentration (0.02 M) is about a factor of 500 lower than that of the solvent. It should also be noted that the measured $\text{Re}(\chi^{(3)})$ values can be either positive or negative depending on the solvent and the measurement wavelength.

The NLO properties (nonlinear absorption and induced refractive index change) of a chromophore solution are mainly determined by three factors: (1) chromophore molecular structure, (2) solvent effects, and (3) resonant enhancement, which depends on the laser measurement wavelength. The two types of resonant enhancement are one-photon and two-photon (see eq S1), with the former determined by linear absorption spectral properties, and the latter by two-photon absorption spectral properties, both depending on the laser wavelength. The present NLO measurements show that both $PMe_3TC_6(CN)_2$ and $QMeTC_6(CN)_2$ have negligible nonlinear absorption at ~800 and ~1300 nm (Table 5), whereas $PMe_3TC_6(CN)_2$ clearly shows substantial Re(γ) values versus the pure solvent and the quartz glass standard.

Due to the differences in experimentally measured (Table 2) versus calculated (Table 1) excitation energies, the second hyperpolarizabilities from Z-scan measurements cannot be compared directly with calculated values at the same wavelength. For example, the computed value for $PMe_3TC_6(CN)_2$ in $CHCl_3$ at 775 nm (Table 4) and the experimentally measured value in DCM at 800 nm (Table 5) have opposite signs. This arises because the one-photon resonance of the chromophore in DCM is at ~634 nm (blue-shifted relative to 800 nm), whereas the calculated value is ~1033 nm (red-shifted relative to 775 nm). A more practical comparison between theory and experiment can be made between the measured value at 800 nm of -1.42×10^{-32} esu and the calculated value at 1300 nm of -2.58×10^{-32} esu, because these wavelengths are comparably red-shifted relative to the respective one-photon resonance wavelengths. These values are of the right sign and the same order of magnitude, showing good agreement between theory and experiment.

Table 6 compares the nonlinear refractive index performance of three recently reported twisted chromophores with other types of organic NLO chromophores measured under similar Z-scan conditions (at somewhat different wavelengths). When compared with other twisted π-systems in DCM, $PMe_3TC_6(CN)_2$ shows a second hyperpolarizability that is more than

DOI: 10.1021/jacs.5b12457
J. Am. Chem. Soc. 2016, 138, 6975−6984

twice that of Cy-TICT,[22] and more than 10 times that of TMC-2.[20] Its second hyperpolarizability compares well with cationic dye 1a[41] and ST1,[42] which have significantly larger π-systems than the condensed donor−acceptor structure of $PMe_3TC_6(CN)_2$. These results show that $PMe_3TC_6(CN)_2$ in DCM is a promising candidate for optical switching, and data storage and transmission applications in the ∼800 nm spectral range. In this case the laser wavelength is located at the red edge of the strong one-photon absorption band, and is situated on the blue-edge of the corresponding two-photon absorption band. Therefore, one- and/or two-photon resonant enhancement may contribute to the measured nonlinearity. The T parameter for $PMe_3TC_6(CN)_2$ is the smallest among the studied twist motif chromophores, indicating a great potential for aforementioned applications. Note also that γ values of $\sim 10^{-34}$ esu have been reported from terthiophene and quaterthiophene,[43] and γ values of $\sim 10^{-31}$ esu have been obtained for some π-extended polymethine systems.[16]

CONCLUSION

In a series of twisted molecular donor−acceptor π-systems, the structural and electronic effects of: (1) an electron-rich, less aromatic thiophene ring on the donor subfragment, (2) increasing annelation of arene rings at the acceptor subfragment pyridine core, and (3) inter-aryl twist were studied to expand the tictoid chromophore design paradigm. Efficient synthetic access to these thiophene-based chromophores was developed by combining multiple required structural elements in one synthon (3-hexylthiophene). Spectroscopic characterization supported by theoretical calculations shows that the degree of substitution around the donor−acceptor inter-aryl linkage dictates the twist angle, and thereby charge delocalization across the π-system. FTIR, NMR, and optical spectroscopies enabled rigorous analysis of chromophore π-electron distribution in solution and in the solid state, and show that the balance between the ZA and NQ forms varies with the chromophore environment. The most highly substituted systems have the largest calculated twist angles, and favor the ZA forms due to their limited ability to delocalize charges across the π-system. However, acceptor core arene ring annelation imparts aromatic stability to the NQ structure despite the steric strain. Balancing these two factors enables some chromophores to adopt exceptionally medium-responsive ground-state structures. Incorporation of a thiophene unit in these chromophores permits substantial charge separation and ground-state dipole moments despite twist angles that are ∼20° smaller than those of TMC systems. The smaller twist angles enhance ICT transition dipoles, while thiophene's reduced aromaticity and higher electron density raise HOMOs and compress energy gaps. Experimental and computational comparisons between the high-twist $PMe_3TC_6(CN)_2$ and the moderately twisted $QMeTC_6(CN)_2$ reveal strong correlations of second hyperpolarizabilities with inter-aryl twist angles. In these tictoid systems, cooperative enhancement of the third-order nonlinearity due to the coupling of ICT and close-lying excited states ultimately produces NLO properties with possibilities for use in optical-switching applications: negligible nonlinear absorptivity with large nonlinear refractive index changes. In particular, $PMe_3TC_6(CN)_2$ shows resonance-enhanced third-order nonlinear responses comparable to those of other recently reported tictoid chromophores.

ASSOCIATED CONTENT

Supporting Information

The Supporting Information is available free of charge on the ACS Publications website at DOI: 10.1021/jacs.5b12457.

Experimental methods, synthetic details, structural characterizations, calculations of molecular parameters, and aggregation studies (PDF)

AUTHOR INFORMATION

Corresponding Authors

*pnprasad@buffalo.edu
*t-marks@northwestern.edu
*reynolds@chemistry.gatech.edu

Notes

The authors declare no competing financial interest.

ACKNOWLEDGMENTS

We thank the Air Force Office of Scientific Research (Grant FA9550-11-1-0121 and MURI Grant FA-95501410040) for support of this work.

REFERENCES

(1) Prasad, P. N.; Reinhardt, B. A. *Chem. Mater.* **1990**, *2*, 660.
(2) Cho, M. J.; Choi, D. H.; Sullivan, P. A.; Akelaitis, A. J. P.; Dalton, L. R. *Prog. Polym. Sci.* **2008**, *33*, 1013.
(3) Sullivan, P. A.; Dalton, L. R. *Acc. Chem. Res.* **2010**, *43*, 10.
(4) Dalton, L. R.; Sullivan, P. A.; Bale, D. H. *Chem. Rev.* **2010**, *110*, 25.
(5) Bredas, J. L.; Adant, C.; Tackx, P.; Persoons, A.; Pierce, B. M. *Chem. Rev.* **1994**, *94*, 243.
(6) Gieseking, R. L.; Mukhopadhyay, S.; Risko, C.; Marder, S. R.; Brédas, J.-L. *Adv. Mater.* **2014**, *26*, 68.
(7) Kuzyk, M. G. *J. Mater. Chem.* **2009**, *19*, 7444.
(8) Bosshard, C.; Sutter, K.; Pretre, P.; Hulliger, J.; Florsheimer, M.; Kaatz, P.; Gunter, P. In *Advances in Nonlinear Optics*; Garito, A. F., Ed.; Gordon and Breach: Basel, Switzerland, 1995; Vol. *1*.
(9) Hermann, J. P.; Ricard, D.; Ducuing, J. *Appl. Phys. Lett.* **1973**, *23*, 178.
(10) Hermann, J. P.; Rustagi, K. C.; Ducuing, J. *IEEE J. Quantum Electron.* **1974**, *10*, 769.
(11) Hermann, J. P.; Ducuing, J. *J. Appl. Phys.* **1974**, *45*, 5100.
(12) Geskin, V. M.; Brédas, J. L. *J. Chem. Phys.* **1998**, *109*, 6163.
(13) Oudar, J. L. *J. Chem. Phys.* **1977**, *67*, 446.
(14) Albert, I. D. L.; Marks, T. J.; Ratner, M. A. *J. Am. Chem. Soc.* **1997**, *119*, 6575.
(15) Marder, S. R.; Cheng, L.-T.; Tiemann, B. G.; Friedli, A. C.; Blanchard-Desce, M.; Perry, J. W.; Skindhøj, J. *Science* **1994**, *263*, 511.
(16) Hales, J. M.; Matichak, J.; Barlow, S.; Ohira, S.; Yesudas, K.; Bredas, J. L.; Perry, J. W.; Marder, S. R. *Science* **2010**, *327*, 1485.
(17) Albert, I. D. L.; Marks, T. J.; Ratner, M. A. *Chem. Mater.* **1998**, *10*, 753.
(18) Albert, I. D. L.; Marks, T. J.; Ratner, M. A. *J. Am. Chem. Soc.* **1997**, *119*, 3155.
(19) Albert, I. D. L.; Marks, T. J.; Ratner, M. A. *J. Am. Chem. Soc.* **1998**, *120*, 11174.
(20) Kang, H.; Facchetti, A.; Jiang, H.; Cariati, E.; Righetto, S.; Ugo, R.; Zuccaccia, C.; Macchioni, A.; Stern, C. L.; Liu, Z.; Ho, S.-T.; Brown, E. C.; Ratner, M. A.; Marks, T. J. *J. Am. Chem. Soc.* **2007**, *129*, 3267.
(21) He, G. S.; Zhu, J.; Baev, A.; Samoc, M.; Frattarelli, D. L.; Watanabe, N.; Facchetti, A.; Agren, H.; Marks, T. J.; Prasad, P. N. *J. Am. Chem. Soc.* **2011**, *133*, 6675.
(22) Shi, Y.; Lou, A. J. T.; He, G. S.; Baev, A.; Swihart, M. T.; Prasad, P. N.; Marks, T. J. *J. Am. Chem. Soc.* **2015**, *137*, 4622.

DOI: 10.1021/jacs.5b12457
J. Am. Chem. Soc. 2016, 138, 6975−6984

(23) Rao, V. P.; Jen, A. K. Y.; Wong, K. Y.; Drost, K. J. *Tetrahedron Lett.* **1993**, *34*, 1747.
(24) Abbotto, A.; Beverina, L.; Bradamante, S.; Facchetti, A.; Klein, C.; Pagani, G. A.; Redi-Abshiro, M.; Wortmann, R. *Chem. - Eur. J.* **2003**, *9*, 1991.
(25) Stegeman, G. I.; Wright, E. M.; Finlayson, N.; Zanoni, R.; Seaton, C. T. *J. Lightwave Technol.* **1988**, *6*, 953.
(26) Mizrahi, V.; Saifi, M. A.; Andrejco, M. J.; DeLong, K. W.; Stegeman, G. I. *Opt. Lett.* **1989**, *14*, 1140.
(27) Abbotto, A.; Bradamante, S.; Facchetti, A.; Pagani, G. A. *J. Org. Chem.* **1997**, *62*, 5755.
(28) Barder, T. E.; Walker, S. D.; Martinelli, J. R.; Buchwald, S. L. *J. Am. Chem. Soc.* **2005**, *127*, 4685.
(29) Dai, C.; Fu, G. C. *J. Am. Chem. Soc.* **2001**, *123*, 2719.
(30) Su, W.; Urgaonkar, S.; McLaughlin, P. A.; Verkade, J. G. *J. Am. Chem. Soc.* **2004**, *126*, 16433.
(31) Billingsley, K.; Buchwald, S. L. *J. Am. Chem. Soc.* **2007**, *129*, 3358.
(32) Juchnovski, I. N.; Radomirska, V. B.; Binev, I. G.; Grekova, E. A. *J. Organomet. Chem.* **1977**, *128*, 139.
(33) McRae, E. G. *J. Phys. Chem.* **1957**, *61*, 562.
(34) Grabowski, Z. R.; Rotkiewicz, K.; Rettig, W. *Chem. Rev.* **2003**, *103*, 3899.
(35) Manohara, S. R.; Kumar, V. U.; Shivakumaraiah; Gerward, L. *J. Mol. Liq.* **2013**, *181*, 97.
(36) Wang, Y. L.; Frattarelli, D. L.; Facchetti, A.; Cariati, E.; Tordin, E.; Ugo, R.; Zuccaccia, C.; Macchioni, A.; Wegener, S. L.; Stern, C. L.; Ratner, M. A.; Marks, T. J. *J. Phys. Chem. C* **2008**, *112*, 8005.
(37) Keinan, S.; Zojer, E.; Bredas, J. L.; Ratner, M. A.; Marks, T. J. *J. Mol. Struct.: THEOCHEM* **2003**, *633*, 227.
(38) Isborn, C. M.; Davidson, E. R.; Robinson, B. H. *J. Phys. Chem. A* **2006**, *110*, 7189.
(39) Sheik-Bahae, M.; Said, A. A.; Wei, T. H.; Hagan, D. J.; Van Stryland, E. W. *IEEE J. Quantum Electron.* **1990**, *26*, 760.
(40) Samoc, M.; Samoc, A.; Humphrey, M. G.; Cifuentes, M. P.; Luther-Davies, B.; Fleitz, P. A. *Mol. Cryst. Liq. Cryst.* **2008**, *485*, 894.
(41) Lin, H.-C.; Kim, H.; Barlow, S.; Hales, J. M.; Perry, J. W.; Marder, S. R. *Chem. Commun.* **2011**, *47*, 782.
(42) Attias, A.-J.; Cavalli, C.; Lemaître, N.; Chérioux, F.; Maillotte, H.; Ledoux, I.; Zyss, J. *J. Opt. A: Pure Appl. Op.* **2002**, *4*, S212.
(43) Zhao, M. T.; Singh, B. P.; Prasad, P. N. *J. Chem. Phys.* **1988**, *89*, 5535.

DOI: 10.1021/jacs.5b12457
J. Am. Chem. Soc. 2016, 138, 6975−6984